

## **Adsorption of selenium(VI) onto nano transition alumina**

Jordan, N.; Franzen, C.; Lützenkirchen, J.; Foerstendorf, H.; Hering, D.; Weiss, S.;  
Heim, K.; Brendler, V.;

Originally published:

June 2018

**Environmental Science: Nano 5(2018)7, 1661-1669**

DOI: <https://doi.org/10.1039/c8en00293b>

Perma-Link to Publication Repository of HZDR:

<https://www.hzdr.de/publications/Publ-27204>

Release of the secondary publication  
on the basis of the German Copyright Law § 38 Section 4.

# Uptake of selenium(VI) onto nano transition alumina

Norbert Jordan<sup>1,\*</sup>, Carola Franzen<sup>1</sup>, Johannes Lützenkirchen<sup>2</sup>, Harald Foerstendorf<sup>1</sup>,

David Hering<sup>1,3</sup>, Stephan Weiss<sup>1</sup>, Karsten Heim<sup>1</sup>, Vinzenz Brendler<sup>1</sup>

<sup>1</sup>Helmholtz-Zentrum Dresden - Rossendorf (HZDR), Institute of Resource Ecology, Bautzner  
Landstraße 400, 01328 Dresden (Germany)

<sup>2</sup>Institute for Nuclear Waste Disposal, Karlsruhe Institute of Technology, Hermann-von-  
Helmholtz Platz 1, 76344 Eggenstein-Leopoldshafen (Germany)

<sup>3</sup>current affiliation: sunfire GmbH

Gasanstaltstraße 2, 01237 Dresden, Germany

\*Corresponding author:

Phone: +49 351 260 2148, e-mail: [n.jordan@hzdr.de](mailto:n.jordan@hzdr.de)

18 **Abstract**

19 The adsorption of selenium(VI) onto nano transition alumina ( $\gamma/\delta\text{-Al}_2\text{O}_3$ ) was investigated at  
20 both macroscopic and molecular levels. The uptake of selenium(VI) was found to decrease upon  
21 increasing pH (5-10) and ionic strength (0.01-0.1 mol·L<sup>-1</sup>). At the molecular level, *in situ*  
22 attenuated total reflection Fourier-transform infrared (ATR FT-IR) spectroscopy established the  
23 predominant formation of a bidentate outer-sphere surface complex throughout the investigated  
24 pH range. The acid-base surface properties of transition alumina (surface charge) together with  
25 the Se(VI) adsorption edges were successfully described using a 1-pK with charge distribution  
26 surface complexation model and one outer-sphere surface species, namely  
27  $\{(\equiv\text{AlOH}_2^{+0.5})_2\text{SeO}_4^{2-}\}$ , according to the IR studies. These new spectroscopic results can be  
28 implemented in reactive transport models to enable a more consistent and trustworthy prognostic  
29 modeling of the environmental fate of selenium(VI).

30  
31 **KEYWORDS:** Selenium(VI); transition alumina; sorption; *in situ* ATR FT-IR spectroscopy;  
32 surface complexation modeling

33

## 34 **Introduction**

35 Selenium is an essential element with toxic effects when high concentrations ( $>400 \mu\text{g}\cdot\text{d}^{-1}$ ) of  
36 bioaccessible species are incorporated.<sup>1, 2</sup> Mines, coal-fired power plants, oil refineries, and  
37 agriculture are important sources of anthropogenic Se dissemination, generating contaminated  
38 waters and wastewaters.<sup>3, 4</sup> Selenium is a potential pollutant of water bodies, its concentration has  
39 to be monitored in drinking-water and in wastewaters. Besides its potential chemotoxicity, the  
40 <sup>79</sup>Se isotope is also an important issue, since it contributes to the radiation inventory of a potential  
41 nuclear waste repository due to its long half-life ( $\sim 3.27 \times 10^5$  years).<sup>5</sup> Detailed knowledge about  
42 selenium speciation and the resulting mobility and bioavailability is therefore of great importance  
43 for both the treatment of Se-contaminated wastewater and the safe disposal of radioactive waste.

44 Selenate ( $\text{Se(VI)O}_4^{2-}$ ) is the predominant aqueous species under most natural redox  
45 conditions.<sup>1, 2</sup> One major process controlling the mobility of selenium in the environment is the  
46 adsorption onto mineral surfaces. Aluminum oxides are among the most abundant and reactive  
47 minerals found in soils and sediments.<sup>6</sup> In addition, they are widely involved in the industry, e.g.  
48 for catalytic processes<sup>7-9</sup> due to their high surface area. Aluminum oxides have been traditionally  
49 used as model oxides to understand the reactivity of clay minerals, since their aluminol surface  
50 groups exhibit similar behavior compared to those at the edges of clays.<sup>10</sup> They have also been  
51 used in laser-induced luminescence spectroscopy studies as analogues for iron oxides.<sup>11, 12</sup>

52 At the macroscopic level, the adsorption of selenium(VI) by  $\gamma\text{-Al}_2\text{O}_3$ ,  $\delta\text{-Al}_2\text{O}_3$ , gibbsite and  
53 aluminum hydroxide has been investigated.<sup>6, 13-20</sup> For the geochemical modeling of adsorption  
54 processes occurring at the water-mineral interface via surface complexation models (SCMs), a  
55 comprehensive knowledge derived from spectroscopic investigations on the surface speciation is

56 mandatory. The formation of non-protonated outer-sphere surface complexes during  
 57 selenium(VI) sorption onto  $\gamma$ -Al<sub>2</sub>O<sub>3</sub> (pH range 4-7), onto hydrous aluminum oxide (pH range 3.5-  
 58 6.0) and onto hydrated  $\gamma$ -Al<sub>2</sub>O<sub>3</sub> surface (pH range 4-7.6) was evidenced by IR, Raman, and  
 59 EXAFS spectroscopy.<sup>6, 16, 21</sup> Though the presence of a small fraction of inner-sphere complexes  
 60 onto  $\gamma$ -Al<sub>2</sub>O<sub>3</sub> at pH < 6 was detected,<sup>21</sup> it was only suggested on hydrous aluminum oxide (pH  
 61 range 3.5-6).<sup>16</sup>

62 Few studies dealing with surface complexation modeling of selenate adsorption on alumina  
 63 phases are currently available in the literature, based on the diffuse layer model<sup>22</sup> and the triple  
 64 layer model<sup>15, 23</sup>. Ghosh et al.<sup>23</sup> considered the two surface species  $\{\equiv\text{AlOH}_2^+-\text{HSeO}_4^-\}$  and  
 65  $\{\equiv\text{AlOH}_2^+-\text{SeO}_4^{2-}\}$ , Wu et al.<sup>15</sup> only  $\{\equiv\text{AlOH}_2^+-\text{SeO}_4^{2-}\}$ , while Wang et al.<sup>22</sup> proposed the three  
 66 species  $\{\equiv\text{AlOH}_2-\text{SeO}_4\}^-$ ,  $\{\equiv\text{AlOH}_2-\text{H}_2\text{SeO}_4\}^+$  and  $\{\equiv(\text{AlO})_2-\text{SeO}_4\}^{4-}$ . None of them  
 67 constrained the number of species as well as their density by spectroscopic evidence. It thus  
 68 appears that an accurate description of selenium(VI) adsorption on alumina phases via SCMs is  
 69 currently missing.

70 The goal of this study was to provide a thorough understanding of the adsorption mechanism of  
 71 Se(VI) onto nano transition alumina. The thermodynamically stable phase of alumina is  $\alpha$ -Al<sub>2</sub>O<sub>3</sub>,  
 72 and other polymorphs such as  $-\gamma$ ,  $-\delta$ , and  $-\eta$  are metastable and usually designed as transition  
 73 alumina. The oxides are less stable than oxyhydroxides or hydroxides. As a consequence, the  
 74 surface and bulk properties of the adsorbent have to be controlled, which was achieved in the  
 75 present work by combining X-ray diffraction (XRD), potentiometric titrations and zeta potential  
 76 measurements. The macroscopic modelling requires batch sorption data, recorded under different  
 77 pH, ionic strength and initial Se(VI) concentration conditions. The thermodynamic based  
 78 description of sorption processes at the solid-water interface based on SCMs has to rely on a

79 thorough description of the number of species at the surface, their stoichiometry and denticity,  
80 their binding strength as well as their reversibility. This can be achieved by applying advanced  
81 spectroscopic techniques such as attenuated total reflection Fourier-transform infrared (ATR FT-  
82 IR) spectroscopy. Indeed, the latter provides a detailed knowledge at the molecular level of the  
83 structure of the surface species and permits to follow *in situ* adsorption processes within the sub-  
84 minute range, even for micro-molar concentration ranges. Exactly this comprehensive  
85 combination of methods was exploited in this study.

86

## 87 **Experimental**

### 88 **Reagents**

89 The background electrolyte NaCl solutions were prepared from a Merck powder (p.a.) in  
90 deionized water (Milli-Q, 18.2 M $\Omega$ ·cm). Selenium(VI) stock solutions (0.1 mol·L<sup>-1</sup>) were  
91 prepared by dissolving Na<sub>2</sub>SeO<sub>4</sub> (Sigma Aldrich, p.a.) in deionized water (Milli-Q, 18.2 M $\Omega$ ·cm).  
92 All experiments were carried out using diluted fractions of these solutions and CO<sub>2</sub>-free  
93 deionized water. In order to avoid possible contamination of the solutions by silicate, and in  
94 parallel to minimize container wall adsorption, polypropylene or polycarbonate flasks were used  
95 in all experiments.

### 96 **Characterization of nano transition Al<sub>2</sub>O<sub>3</sub>**

97 Al<sub>2</sub>O<sub>3</sub> was purchased from Alfa Aesar (No. 44931, 99.5 % purity specified by the supplier).  
98 The particle size ranges between 40 and 50 nm according to the manufacturer. The specific  
99 surface area (SSA) was determined to be 37 m<sup>2</sup>·g<sup>-1</sup> by the Brunauer–Emmet–Teller (BET)  
100 equation with nitrogen adsorption isotherms at 77 K (Multi-point Beckman Coulter analyzer SA  
101 3100). Minor impurities of approx. 20  $\mu\text{g}\cdot\text{g}^{-1}$  for Mg, Cu, and W, 120  $\mu\text{g}\cdot\text{g}^{-1}$  for Fe and  
102 550  $\mu\text{g}\cdot\text{g}^{-1}$  for Ca were observed by inductively coupled plasma-mass spectrometry (ICP-MS,  
103 ELAN 9000 Perkin Elmer) after digestion of the mineral. XRD measurements revealed the  
104 presence of both  $\gamma$ -Al<sub>2</sub>O<sub>3</sub> (ICDD 00–002–1420) and  $\delta$ -Al<sub>2</sub>O<sub>3</sub> (ICDD 00–056–1186) in a ratio of  
105 approximately 30:70 (Figure S1, Supporting Information (SI)). No detectable impurities (> 5 %  
106 w/w) of other aluminum phases such as e.g. gibbsite or bayerite were observed in the raw  
107 material.

108 In order to check potential phase transformation of transition- $\text{Al}_2\text{O}_3$ , samples (mass to volume  
109 ratio  $m/v = 0.5 \text{ g}\cdot\text{L}^{-1}$ ) were suspended in  $0.1 \text{ mol}\cdot\text{L}^{-1}$  NaCl aqueous solutions with pH values  
110 ranging from 4 to 12 (adjusted with  $0.1$  and  $0.01 \text{ mol}\cdot\text{L}^{-1}$  HCl and NaOH), in a glove box under  
111 anoxic conditions ( $\text{N}_2$  atmosphere,  $\text{O}_2 < 10$  ppm). The pH measurements (pH-meter Inolab WTW  
112 series pH720) were performed using a combination glass electrode (BlueLine 16 pH, Schott  
113 Instruments) with a Ag/AgCl reference electrode, to an accuracy of  $\pm 0.05$ . Electrodes were  
114 calibrated using three NIST-traceable buffer solutions from WTW (pH 1.679, pH 4.006 and pH  
115 6.865, each value for  $25 \text{ }^\circ\text{C}$ ). After 16 days of equilibration at room temperature with regular pH  
116 adjustment, the samples were centrifuged and subsequently lyophilized. Afterwards the samples  
117 were also characterized by XRD. Additionally, the solubility of transition- $\text{Al}_2\text{O}_3$  was checked on  
118 the same samples ( $m/v = 0.5 \text{ g}\cdot\text{L}^{-1}$ , 16 days of shaking,  $0.1 \text{ mol}\cdot\text{L}^{-1}$  NaCl). For this, the  
119 supernatants of the batch experiments after phase separation were analyzed by ICP-MS in order  
120 to derive the concentration of dissolved aluminum.

121 The impact of pH (from 3.5 to 11), and duration of mineral ageing in suspension (one hour to  
122 four weeks) on the zeta potential of transition alumina ( $m/v = 0.2 \text{ g}\cdot\text{L}^{-1}$ ,  $0.1 \text{ mol}\cdot\text{L}^{-1}$  NaCl) was  
123 evaluated at  $25 \text{ }^\circ\text{C}$  using a Laser-Doppler-Electrophoresis instrument (nano-ZS, Malvern  
124 Instruments Ltd.). The results are shown in Figure S2 in the SI.

125 The surface acid-base properties of nano transition alumina were characterized by  
126 potentiometric titrations and zeta potential studies. Potentiometric titrations (pH range 5 to 9.5)  
127 were performed at different ionic strengths of NaCl ( $0.1$ ,  $0.05$  and  $0.01 \text{ mol}\cdot\text{L}^{-1}$ ) with a Metrohm  
128 736 GP Titrino titrator, at a mass to volume ratio of  $30 \text{ g}\cdot\text{L}^{-1}$  under Ar atmosphere (SI). This high  
129 solid to liquid ratio minimizes the effects of solubility relative to the surface reactions. Zeta



130 potential measurements were performed under CO<sub>2</sub> exclusion, at m/v = 0.25 g·L<sup>-1</sup> and at two  
131 ionic strengths (0.005 and 0.01 mol·L<sup>-1</sup> NaCl).

### 132 **Batch Sorption experiments**

133 The impact of pH and ionic strength on the sorption of Se(VI) onto alumina was studied in the  
134 pH range from 5 to 10 at room temperature. The mass to volume ratio was 0.5 or 1 g·L<sup>-1</sup>. All  
135 sorption experiments were performed in a glove box under anoxic conditions (N<sub>2</sub> atmosphere,  
136 O<sub>2</sub> < 10 ppm). The suspensions were equilibrated for 3 days in a head-over-head shaker (with pH  
137 adjustment). Required amounts of selenium(VI) were added to reach a concentration of 1 ×  
138 10<sup>-5</sup> mol·L<sup>-1</sup> or 2 × 10<sup>-5</sup> mol·L<sup>-1</sup> and the suspensions were shaken for 2 more days, which made  
139 sure that constant uptake was achieved, since a time-dependent study (data not shown) indicated  
140 a plateau of the sorption process reached after a contact time of less than 24 h. pH measurements  
141 were performed as already described above. At the end of the sorption stage, the samples were  
142 centrifuged at 12,000 × g for 2 h (Sigma 3-30KH centrifuge). Scattered light intensity  
143 measurements (BI-90 particle sizer, Brookhaven Instruments) were used to ensure that  
144 supernatants were free of colloids. The selenium concentration in the supernatant, determined by  
145 ICP-MS, was used to calculate the amount of adsorbed selenium(VI). Se uptake on the walls of  
146 polypropylene vials was found to be negligible. Additionally, zeta potential measurements were  
147 performed under CO<sub>2</sub>-exclusion, using a m/v of 0.25 g·L<sup>-1</sup>, an ionic strength of 0.01 mol·L<sup>-1</sup> and  
148 an initial Se(VI) concentration of 1 × 10<sup>-4</sup> mol·L<sup>-1</sup>.

### 149 **IR Spectroscopy**

150 The IR experiments were carried out with a Bruker Vertex 80/v spectrometer, equipped with a  
151 horizontal ATR diamond crystal accessory (SamplIR II, Smiths Inc., 9 reflections, angle of

152 incidence: 45°) and a Mercury Cadmium Telluride (MCT) detector. Each IR spectrum was an  
153 average over 256 scans at a spectral resolution of 4 cm<sup>-1</sup> using the OPUS<sup>TM</sup> software for data  
154 acquisition and evaluation.

155 The sample compartment was purged with dry air. To minimize interferences between the  
156 strong absorption band of H<sub>2</sub>O below 1000 cm<sup>-1</sup> and the potential SeO<sub>4</sub><sup>2-</sup> bands arising from  
157 adsorption (between 900 and 700 cm<sup>-1</sup>), all studies were performed in D<sub>2</sub>O. All solutions were  
158 prepared and measured in N<sub>2</sub> atmosphere to prevent CO<sub>2</sub> interference and fast exchange between  
159 hydrogen and deuterium. The pH of the selenium working solution, measured using electrodes  
160 calibrated with aqueous buffers as described above, was adjusted with 0.1 mol L<sup>-1</sup> NaOD and  
161 DCl. pD values were then calculated from pH values using the equation pD = pH + 0.4.<sup>24</sup> The  
162 determination of the selenium sorption mechanisms onto transition alumina was analogous to  
163 earlier spectroscopic adsorption studies.<sup>25-28</sup>

164 Briefly, transition alumina was deposited directly on the surface of the diamond crystal from a  
165 2.5 g·L<sup>-1</sup> suspension and dried under a gentle N<sub>2</sub> flow. As a first step, for equilibration of the  
166 mineral film, the cell was rinsed with the background electrolyte (0.1 and 0.01 mol·L<sup>-1</sup> NaCl) for  
167 60 minutes. Transition alumina might provide spectral interferences during the investigation of  
168 Se(VI) adsorption processes, since significant bands between 1000 and 600 cm<sup>-1</sup> are present  
169 (Figure S3 in SI). However, experiments in the presence of the background electrolyte clearly  
170 evidenced the long-term stability of the transition alumina on the ATR cell. Then, the blank  
171 electrolyte solution was replaced by the selenium(VI) solution (5 × 10<sup>-7</sup> mol·L<sup>-1</sup>) for 2 hours, to  
172 study the adsorption processes. As a last step, the film was rinsed again with a blank solution for  
173 60 minutes to study the potential desorption of selenium(VI) from the transition alumina film. All  
174 steps were performed with solutions at constant pD and involved a continuous flow rate of

175 100  $\mu\text{L}\cdot\text{min}^{-1}$  provided by a peristaltic pump. Acquisition of single beam spectra was  
176 continuously accomplished during all steps of the experiment. Spectra reflecting the molecular  
177 processes occurring at the solid-liquid interface were calculated from the single beam spectra  
178 before and during each experimental step according to Lambert-Beer's law.

### 179 **Surface Complexation Modeling**

180 Surface complexation modeling was performed using the charge distribution-multi site  
181 complexation (CD-MUSIC) model with a one-pK approach. To describe the surface properties of  
182 transition alumina, the pragmatic approach used by Mayordomo et al.<sup>28</sup> was followed. One site  
183 representing singly coordinated hydroxyl groups with fractional charges was used, involving a  
184 site density of 7 sites $\cdot\text{nm}^{-2}$ . A pK of 9.3 was used to model the potentiometric titrations and zeta  
185 potential measurements data. A better data description was achieved with the three plane model  
186 in comparison to the Basic Stern model. The adjustable parameters were the two electrolyte  
187 association constants ( $\text{Na}^+$  and  $\text{Cl}^-$ , located at the head-end of the diffuse layer) and the  
188 capacitance value  $C_1$  ( $C_2$  being fixed at 5  $\text{F}\cdot\text{m}^{-2}$ ).<sup>28, 29</sup> The slip-plane distance,  $s$ , was fitted to  
189 obtain a good fit to the zeta potential data.<sup>30</sup> The fitting procedure was performed using a  
190 modified version of FITEQL coupled to UCODE.<sup>31, 32</sup> All activity coefficient treatment was done  
191 using the Davies equation.

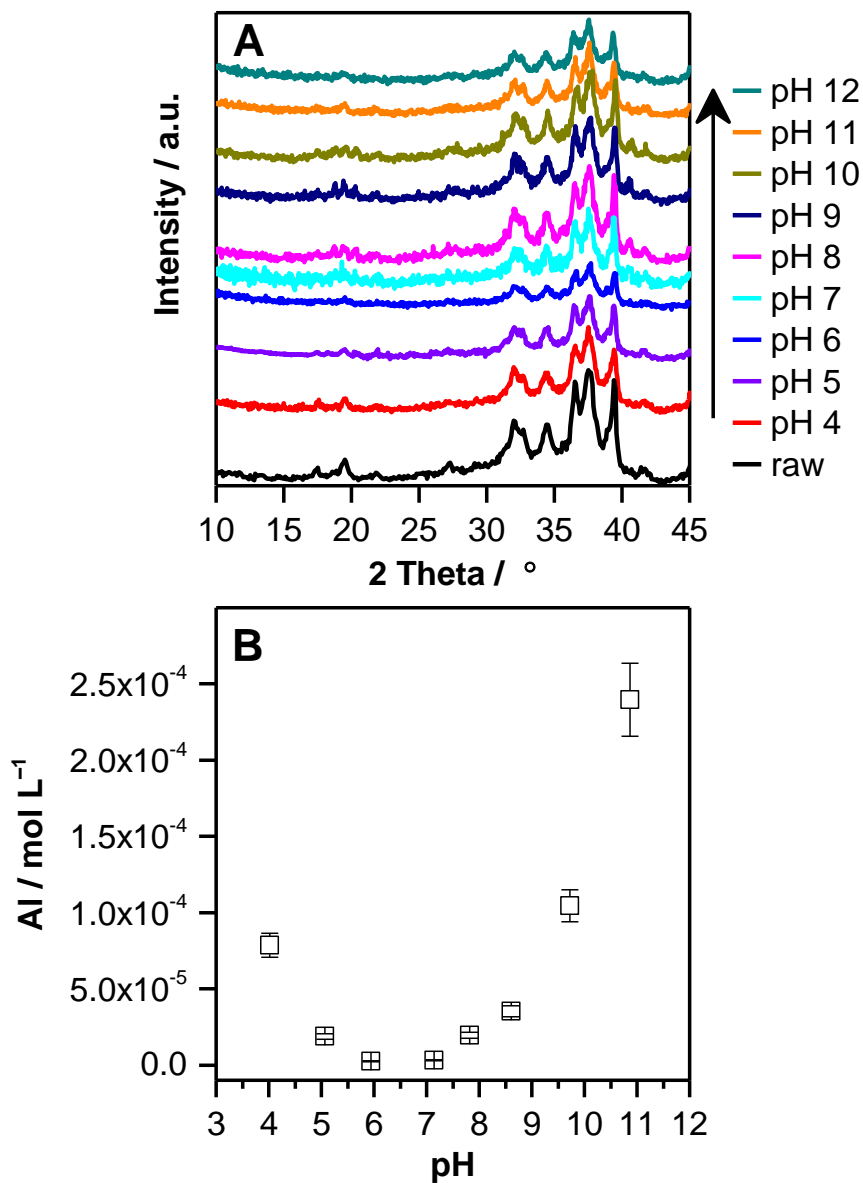
192

193 **Results and discussion**

194 **Surface Acid–base Behavior, Zeta Potentials, and Modeling in the absence of selenate**

195 Several previous studies have shown that  $\gamma$ -Al<sub>2</sub>O<sub>3</sub> in aqueous suspensions transforms into  
196 (oxy)hydroxides even at room temperature and after a few days.<sup>33-37</sup> The pH dependent  
197 investigation of the stability of the bulk transition–Al<sub>2</sub>O<sub>3</sub> by means of XRD shows that during the  
198 equilibration time of 16 days, no transformation to other aluminum-(oxy)-hydroxides, such as  
199 boehmite, gibbsite or bayerite took place (Figure 1A). IR data did not reveal any surface  
200 transformation of nano transition alumina into bayerite or gibbsite even after 1 month. This  
201 observation is in excellent agreement with a previous study by Müller et al.<sup>38</sup> who used exactly  
202 the same charge.

203



204  
 205 **Figure 1.** (A) XRD of transition alumina as a function of pH after 16 days of equilibration at  
 206 room temperature (B) solubility of transition alumina as a function of pH at room temperature  
 207 ( $m/v = 0.5 \text{ g}\cdot\text{L}^{-1}$ , 16 days of shaking,  $0.1 \text{ mol}\cdot\text{L}^{-1}$  NaCl).

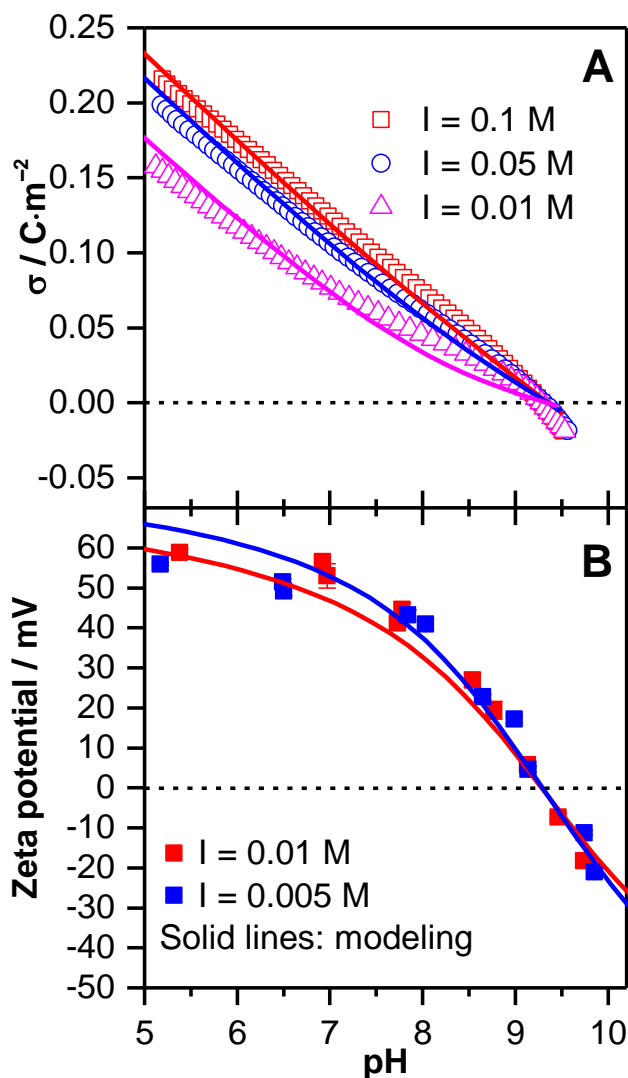
208 The isoelectric point of transition alumina at  $25 \text{ }^\circ\text{C}$  and  $0.1 \text{ mol}\cdot\text{L}^{-1}$  NaCl was found at pH 9.5  
 209 (Figure S2 in SI) irrespective of different equilibration times ranging from a couple of minutes to  
 210 four weeks. This value is in good agreement with literature data of  $\gamma\text{-Al}_2\text{O}_3$ ,<sup>39</sup> whereas no

211 literature exists for  $\delta$ -Al<sub>2</sub>O<sub>3</sub>. These findings suggest that the variable surface charge does not  
212 significantly change, which would rule out ageing processes, in agreement with the spectroscopic  
213 results.

214 The solubility of nano transition alumina was found to increase significantly at pH < 5 and at  
215 pH > 9 (Figure 1B). In order to avoid significant dissolution, batch and zeta potential experiments  
216 were performed from pH 5 to 10. At pH 9-10, Se uptake becomes negligible and is therefore not  
217 impacted by the increased solubility.

218 Self-consistent modeling of the Se(VI) adsorption data requires the knowledge of the acid-base  
219 parameters of the sorbing phase. The experimental titration results (surface charge density vs.  
220 pH) at different ionic strengths are shown in Figure 2A, while zeta potential measurements as a  
221 function of pH are given in Figure 2B. Solid lines represent the modeling results in each figure.

222



223

224 **Figure 2.** (A) Surface charge of the neat surface of transition alumina ( $m/v = 30 \text{ g}\cdot\text{L}^{-1}$ ,  $I = 0.01$ ,  
 225  $0.05$  and  $0.1 \text{ mol}\cdot\text{L}^{-1}$  NaCl, under Ar) ( $\Delta$ ,  $\circ$ ,  $\square$  experiment; — fit). (B) Zeta potential of the  
 226 neat surface of transition alumina ( $m/v = 0.25 \text{ g}\cdot\text{L}^{-1}$ ,  $I = 0.005$  and  $0.01 \text{ mol}\cdot\text{L}^{-1}$  NaCl), under  $\text{N}_2$   
 227 ( $\blacksquare$  experiment; — fit).

228 The surface chemical reactions used and the corresponding constants and required parameters  
 229 are summarized in Table 1. The capacitance  $C_l$  and the parameter  $x$  were  $1.60 \text{ F}\cdot\text{m}^{-2}$  and  $0.33$ ,

230 respectively. The fitted parameter  $x$  is related to the slip plane distance  $s$  and the ionic strength  
 231 dependent Debye length  $\kappa$  by  $x = s \times \kappa$ .<sup>40</sup>

232  
 233 **Table 1.** Parameters for the surface species in the Best-Fit Model (surface acid-base  
 234 properties of nano transition alumina and Se(VI) adsorption).

Surface species	$\Delta z_0$	$\Delta z_1$	$\Delta z_2$	reaction	$\log K^\circ$
Surface acid-base properties					
$\equiv\text{AlOH}^{-0.5}$	0	0	0		0
$\equiv\text{AlOH}_2^{+0.5}$	1	0	0	$\equiv\text{AlOH}^{-0.5} + \text{H}^+ \rightleftharpoons \equiv\text{AlOH}_2^{+0.5}$	9.3
$\equiv\text{AlOH}^{-0.5}\cdots\text{Na}^+$	0	0	1	$\equiv\text{AlOH}^{-0.5} + \text{Na}^+ \rightleftharpoons \equiv\text{AlOH}^{-0.5}\cdots\text{Na}^+$	$-0.3 \pm 0.2$
$\equiv\text{AlOH}^{+0.5}\cdots\text{Cl}^-$	0	0	-1	$\equiv\text{AlOH}_2^{+0.5} + \text{Cl}^- \rightleftharpoons \equiv\text{AlOH}_2^{+0.5}\cdots\text{Cl}^-$	$-0.2 \pm 0.1$
Se(VI) adsorption					
$\{(\equiv\text{AlOH}_2^{+0.5})_2\text{SeO}_4^{2-}\}$	2	-1.7	-0.3	$2(\equiv\text{AlOH}^{-0.5}) + 2\text{H}^+ + \text{SeO}_4^{2-} \rightleftharpoons \{(\equiv\text{AlOH}_2^{+0.5})_2\text{SeO}_4^{2-}\}$	$19.5 \pm 1.0$

235 The titration data can be satisfactorily described with the proposed model, i.e. with one singly  
 236 coordinated surface hydroxyl group and the three plane model (Figure 2A). The  $\text{pH}_{\text{IEP}}$  of nano  
 237 transition alumina was found to be 9.3 and was independent of the NaCl concentration (Figure  
 238 2B). This  $\text{pH}_{\text{IEP}}$  value is in agreement with the literature, with  $\text{pH}_{\text{PZC/IEP}}$  of alumina phases mostly  
 239 ranging from pH 8 to 10.<sup>41, 42</sup> The zeta potential curves and the  $\text{pH}_{\text{IEP}}$  were rather well described  
 240 by the proposed model (Figure 2B). Charge penetration of the electrolyte ions in the plane 0 or 1  
 241 did not significantly improve the quality of both titration and zeta potential fits (i.e. at  $I =$   
 242  $0.01 \text{ mol}\cdot\text{L}^{-1}$  in the circumneutral pH range for the titrations and in the pH range from 5 to 7 for

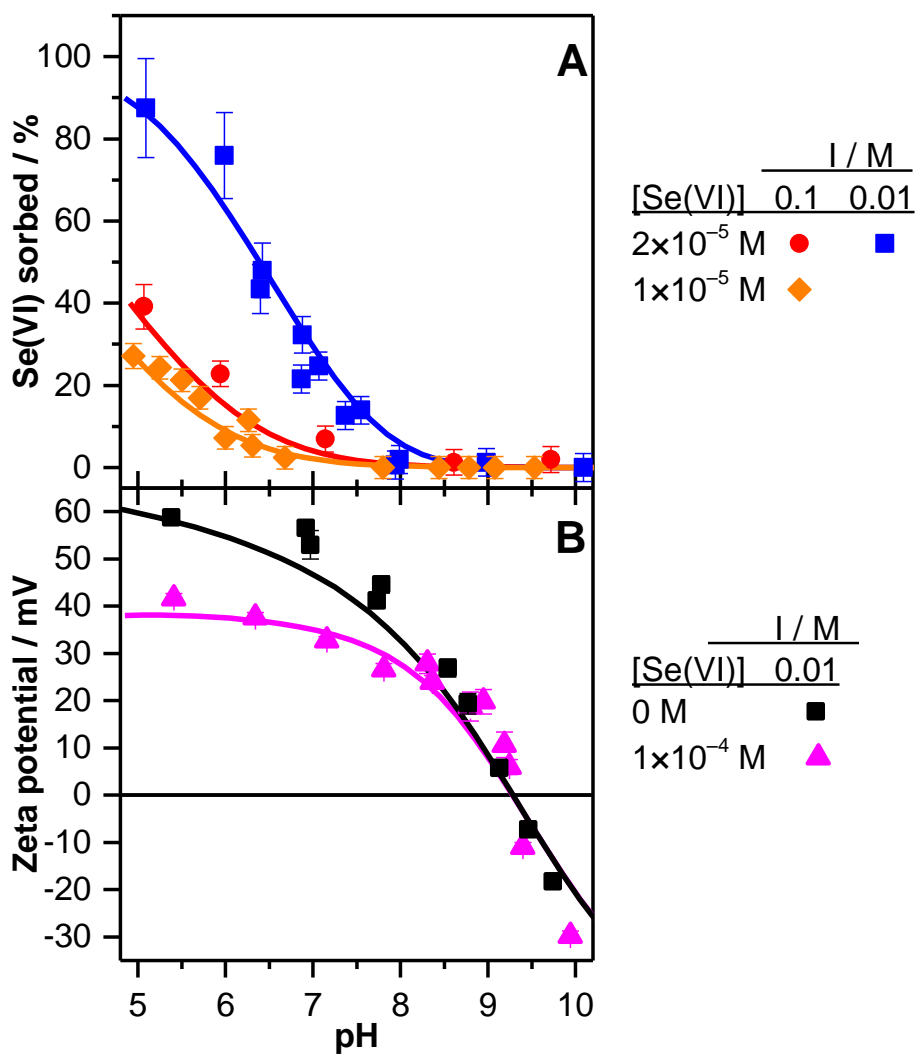


243 the zeta potentials). The model used to calculate the lines in Figure 2 was consequently accepted  
 244 and applied for the modeling of the Se(IV) adsorption data.

245 **Batch and zeta potential studies in the presence of selenate**

246 Batch experiments demonstrated that the adsorption of selenium(VI) onto transition alumina  
 247 was strongly pH-dependent, highest at pH 5 and decreasing with increasing pH (Figure 3A).

248



249

250

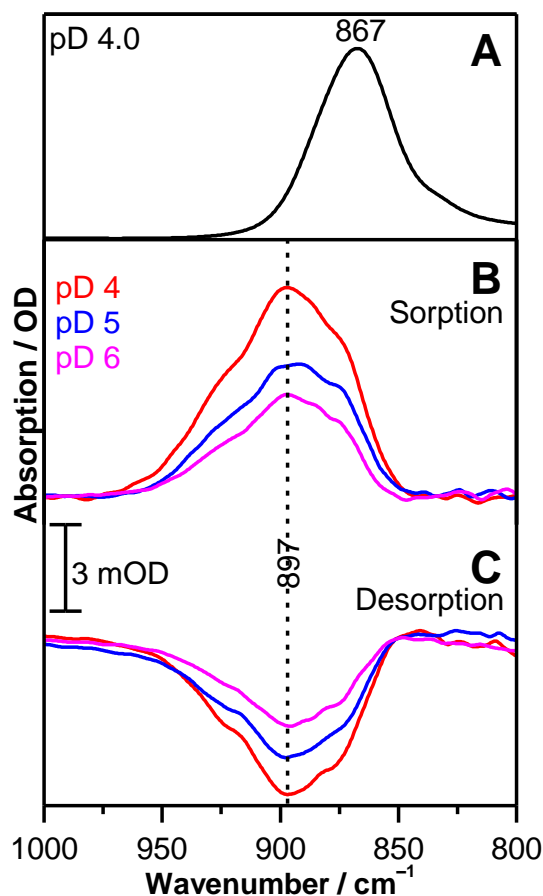
251 **Figure 3.** (A) Se(VI) sorption envelopes onto transition alumina ( $[\text{Se}^{\text{VI}}]_{\text{initial}} = 1 \times$   
 252  $10^{-5} \text{ mol}\cdot\text{L}^{-1}$ ,  $m/v = 0.5 \text{ g}\cdot\text{L}^{-1}$ ,  $I = 0.1 \text{ mol}\cdot\text{L}^{-1}$  NaCl (◆)) and  $[\text{Se}^{\text{VI}}]_{\text{initial}} = 2 \times 10^{-5} \text{ mol}\cdot\text{L}^{-1}$ ,  $m/v =$   
 253  $1 \text{ g}\cdot\text{L}^{-1}$ ,  $I = 0.1 \text{ mol}\cdot\text{L}^{-1}$  NaCl (●) and  $I = 0.01 \text{ mol}\cdot\text{L}^{-1}$  NaCl (■); — fit). (B) Zeta potential of  
 254 the surface of transition alumina ( $[\text{Se}^{\text{VI}}]_{\text{initial}} = 0 \text{ mol}\cdot\text{L}^{-1}$  (■) and  $1 \times 10^{-4} \text{ mol}\cdot\text{L}^{-1}$  (▲),  $m/v =$   
 255  $0.25 \text{ g}\cdot\text{L}^{-1}$ ,  $0.01 \text{ mol}\cdot\text{L}^{-1}$  NaCl). (— fit).

256 This behavior was expected taking into account (i) that the surface charge of transition alumina  
 257 decreased with increasing pH and (ii) that selenium(VI) in solution predominantly exists as  
 258 negatively charged oxyanions. Increasing the ionic strength from 0.01 to 0.1  $\text{mol}\cdot\text{L}^{-1}$  significantly  
 259 reduced the adsorption of Se(VI), indicating competition with background electrolyte ions and/or  
 260 electrostatic effects, suggesting the formation of outer-sphere complexes.<sup>6, 25, 27</sup> From pH 5 to 9,  
 261 the dissolution of alumina was negligible. Indeed, the Al concentration measured in the  
 262 supernatants after the phase separation was not exceeding 5.5 % of the concentration  
 263 corresponding to a theoretical complete dissolution of the sorbing phase. It reached a maximum  
 264 of 14.5 % between pH 9 and 10, but in this pH range the uptake of Se(VI) was already negligible.

265 Upon adsorption of Se(VI), the isoelectric point of transition alumina remained unchanged  
 266 (Figure 3B). However, its zeta potential became less positive at  $\text{pH} < \text{pH}_{\text{IEP}}$ . A similar behavior  
 267 of the  $\text{pH}_{\text{IEP}}$  upon selenium(VI) sorption has been previously reported for  $\gamma\text{-Al}_2\text{O}_3$ ,<sup>6</sup> anatase,<sup>25</sup> and  
 268 maghemite,<sup>27</sup> strongly suggesting the formation of outer-sphere complexes.

### 269 *In situ* ATR FT-IR studies

270 Though solubility experiments revealed increased solubility at  $\text{pH} < 5$ , the *in situ* IR sorption  
 271 experiments were performed at pD 4, 5 and 6 to check potential changes in the adsorption  
 272 mechanism with increasing pH/pD (Figure 4).



273

274 **Figure 4.** (a) IR spectrum of  $0.1 \text{ mol}\cdot\text{L}^{-1}$  selenium(VI) in aqueous solution at  $0.1 \text{ mol}\cdot\text{L}^{-1}$  NaCl  
 275 in  $\text{D}_2\text{O}$ . (b) *In situ* IR spectra taken during selenium(VI) adsorption onto transition alumina  
 276 ( $[\text{Se(VI)}]_{\text{initial}} = 5 \times 10^{-4} \text{ mol}\cdot\text{L}^{-1}$ ,  $\text{D}_2\text{O}$ ,  $0.1 \text{ mol}\cdot\text{L}^{-1}$  NaCl,  $\text{N}_2$ ) recorded after 20 minutes of  
 277 induced sorption at different pD values. (c) *In situ* IR spectra during release of selenium(VI)  
 278 recorded 20 minutes after starting to flush the transition alumina phase with blank solution ( $\text{D}_2\text{O}$ ,  
 279  $0.1 \text{ mol}\cdot\text{L}^{-1}$  NaCl,  $\text{N}_2$ ) at different pD values.

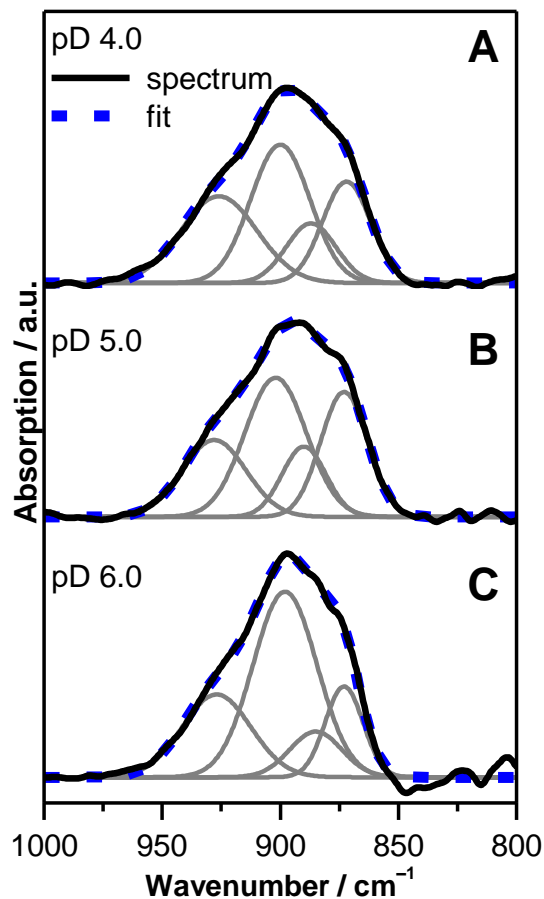
280

281 It was shown that a steady state was achieved within 20 minutes since prolonged exposure to  
 282 Se(VI) up to 120 minutes did not reveal any significant spectral changes (Figures S4, S5 and S6  
 283 in SI).

284 Generally, the amplitudes of the spectra decreased with increasing pD, correlating with the  
285 observations from the batch experiments that the Se(VI) uptake decreases with increasing pH/pD  
286 (Figure 3A). Furthermore, in analogy to the batch experiments, the decrease of Se(VI) sorption  
287 upon increasing the ionic strength from 0.01 to 0.1 mol·L<sup>-1</sup> was spectroscopically exemplarily  
288 reproduced at pD 4 (Figure S7B in SI). Above pD 6, the acquisition of spectra with a reasonable  
289 signal-to-noise ratio became difficult due to the reduced sorption of Se(VI) in this pH range (see  
290 Figure 3A).

291 The interpretation of the vibrational spectra refers to the correlation between the molecule  
292 symmetry and the vibrational modes observed. The tetrahedral SeO<sub>4</sub><sup>2-</sup> anion as it is prevailing in  
293 aqueous solution exhibits two IR active modes, the  $\nu_3$  triply degenerate asymmetric Se–O  
294 stretching and the  $\nu_4$  triply degenerate out of plane O–Se–O bending modes.<sup>43, 44</sup> Since the latter  
295 mode is outside the acquisition range of the MCT detector, only the spectral properties of the  $\nu_3$   
296 mode are considered. In the spectrum of the aqueous SeO<sub>4</sub><sup>2-</sup> ion, a single almost symmetrically  
297 shaped band at 867 cm<sup>-1</sup> is observed reflecting the predominant tetrahedral symmetry of the  
298 aqueous SeO<sub>4</sub><sup>2-</sup> ion (Figure 4A). In contrast, the spectra recorded at pD 4.0, 5.0, and 6.0 after 20  
299 minutes of induced adsorption showed a broad structured band with a maximum around 897 cm<sup>-1</sup>  
300 indicating the occurrence of overlapping bands (Figure 4B).

301  
302 The elucidation of the spectral components contributing to these spectra was achieved by  
303 second derivative spectra. For the spectrum recorded at pD 4, four spectral components were  
304 determined with maxima at 926, 900, 887, and 872 cm<sup>-1</sup>. The fitting result provided a local  
305 residual root-mean-square error ranging from  $5.4 \times 10^{-5}$  to  $9.0 \times 10^{-5}$  (Figure 5A-C).



306  
 307 **Figure 5.** Deconvolution of the IR spectrum of selenium(VI) sorption onto transition alumina  
 308 ( $[\text{Se(VI)}]_{\text{initial}} = 5 \times 10^{-4} \text{ mol}\cdot\text{L}^{-1}$ ,  $\text{D}_2\text{O}$ ,  $0.1 \text{ mol}\cdot\text{L}^{-1} \text{ NaCl}$ , 20 min of sorption,  $\text{N}_2$ ). Dotted line  
 309 indicates the overall fit. (a) pD 4.0, (b) pD 5.0 (c) pD 6.0.

310  
 311 Similar fitting results with only marginally varied frequencies of the peak maxima were  
 312 obtained for the spectra recorded at pD 5 and 6 (Figure 5 B; C) indicating the predominant  
 313 formation of one type of sorption complex on the transition alumina surface throughout this pD  
 314 range.

315 The splitting of the band representing the  $\nu_3(\text{SeO}_4)$  mode into four spectral components can be  
316 interpreted in terms of the reduction of the molecule symmetry from tetrahedral to  $C_{2v}$  as it was  
317 previously observed in our investigation of the sorption processes of Se(VI) onto maghemite.<sup>27</sup>  
318 Intrinsically, lowering the molecule symmetry from  $T_d$  to  $C_{2v}$  leads to the abrogation of the triply  
319 degenerated  $\nu_3$  mode. Additionally, the  $\nu_1$  mode becomes IR active.<sup>27</sup> Hence, the appearance of  
320 four spectral components in the IR spectra of the sorption species strongly suggests the  
321 prevalence of a surface complex showing  $C_{2v}$  symmetry.

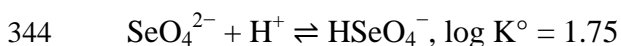
322 Subsequently, desorption was initiated by flushing the flow cell with blank electrolyte solution.  
323 The shapes of spectra exhibited a high congruence to the spectra of the sorption step strongly  
324 suggesting that the same Se(VI) surface species were present during adsorption and release from  
325 the transition alumina surface (Figure 4C). The predominant formation of outer-sphere  
326 complexes can be inferred from the high degree of reversibility over time observed by *in situ*  
327 ATR FT-IR which ranged from ~67 % to ~76 % from pD 4 to 6, as it was observed for other  
328 mineral phases.<sup>25, 27</sup> Additionally, this is in agreement with the results from our batch and zeta  
329 potential experiments (see above). Furthermore, in analogy to the batch experiments, the decrease  
330 of Se(VI) sorption upon increasing the ionic strength from 0.01 to 0.1 mol·L<sup>-1</sup> was  
331 spectroscopically reproduced (Figure S7 in SI). The same spectral characteristics were observed  
332 at pD 4.0 at both 0.1 mol·L<sup>-1</sup> and 0.01 mol·L<sup>-1</sup> NaCl ionic strengths (Figure S7 in SI). In  
333 summary, the vibrational spectroscopic findings clearly demonstrated that selenium(VI) sorption  
334 onto transition alumina proceeds via the predominant formation of bidentate outer-sphere  
335 complexes over the whole pH range investigated.

336

337 **Surface complexation modeling of Se(VI) adsorption processes**

338 The parameters derived from the acid-base model were kept for the Se(VI)-adsorption model,  
 339 implying that the inner and outer-layer capacitances were assumed not to be impacted by the  
 340 adsorption of Se(VI), as well as the slip plane distance. The aqueous Se(VI) protonation constant  
 341 at infinite dilution were taken from the NEA-TDB book for selenium.<sup>45</sup> Only the reaction given  
 342 below is the most relevant for our conditions.

343

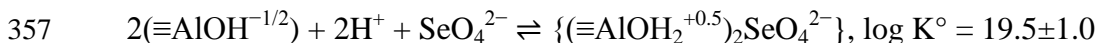


345

346 The formation of one bidentate outer-sphere surface species was derived from the  
 347 spectroscopic studies and implemented in the adsorption model, i.e.  $\{(\equiv\text{AlOH}_2^{+0.5})_2\text{SeO}_4^{2-}\}$  (see  
 348 Table 1). The appropriate formulation of the mass action expression for this bidentate complex  
 349 was performed according to previous recommendations,<sup>46, 47</sup> i.e. by decoupling the mole balance  
 350 and mass balance equations (coefficient 2 only in the matrix B). The location of the charge of the  
 351 Se(VI) ions at the interface was described via the charge distribution (CD) factor. Overall, two  
 352 adjustable parameters were involved: the log K and the concomitant CD-factor. The CD-factors  
 353 can be inferred from Table 1.

354 The adsorption model is summarized in the following reaction equation and the model fit to the  
 355 batch and zeta potential data is shown in Figure 3 (A and B).

356



358

359 A satisfactory description of the adsorption data was obtained (Figure 3A), whatever the initial  
360 concentration of Se(VI) or the ionic strength of the suspensions. The model description of the  
361 zeta potentials of transition alumina in the absence and presence of Se(VI) is shown in Figure 3B.  
362 Overall, the description of the zeta potentials is accurate and the model nicely reproduces the  
363 absence of a  $\text{pH}_{\text{IEP}}$  shift.

364 The location of the Se(VI) charge at the interface was characterized by the best-fit charge  
365 distribution factor. The CD-factor describes how the negative charge of the selenate ion is  
366 distributed in the interfacial layer, i.e. which contribution is going to the 1-plane and the 2-plane.  
367 Most of the charge of the  $\text{SeO}_4^{2-}$  ion is transferred towards the plane 1, leading to a closer  
368 position of the selenate ion to the surface compared to the background electrolyte ions. The free  
369  $\text{SeO}_4^{2-}$  anion has a tetrahedral symmetry and exhibits a bidentate symmetry at the transition  
370 alumina water interface. It is thus conceivable that one of the two remaining oxygens is located  
371 rather close to the surface and one rather oriented towards the solution.

372 The model used to calculate the lines in Figure 3 (A and B) and considering the  $(\equiv\text{AlOH}_2^{+0.5})_2$   
373  $(\text{SeO}_4)^{2-}$  species was the one that yielded the best fit. Since it describes the experimental data  
374 accurately and was in agreement with the spectroscopic observations, other modeling options  
375 (sodium coadsorption, another inner-sphere surface species) were not tested. The published  
376 SCMs studies for Se(VI) adsorption onto alumina involved different stoichiometry and  
377 mechanisms, which makes a direct comparison not suitable.

378



379 **Conclusions**

380 In this study, the adsorption of Se(VI) on transition alumina was shown to decrease upon  
381 increasing pH and ionic strength, leading to a higher Se(VI) mobility under such conditions. At  
382 the molecular level, *in situ* ATR FT-IR spectroscopy identified an outer-spheric bidentate surface  
383 complex as the predominant interfacial Se species over the whole investigated pH range. The  
384 acid-base surface properties as well as the Se(VI) adsorption processes could be successfully  
385 described using a 1-pK model with charge distribution, considering one single species as inferred  
386 from the IR studies. The data derived from this study will be implemented into a sorption  
387 database which is mandatory for safety assessments and for the prediction of Se(VI) fate in the  
388 environment. The evidenced outer-sphere adsorption mechanism associated to fast kinetics and  
389 high reversibility would lead to Se(VI) retardation. However, the lack of irreversibility of the  
390 adsorption process might not be sufficient for preventing Se(VI) leaching and transport in the  
391 environment. If bound to nano alumina as a carrier, filtration or adhesion of the nano particles  
392 would mean that selenate can be re-mobilized, unlike irreversibly bound inner-sphere surface  
393 complexes.

394

395 **Conflicts of interest**

396 The authors declare no competing financial interest.

397 **Acknowledgements**

398 This work is part of the VESPA project, funded by the German Federal Ministry of Economics  
399 and Technology (BMWi) through contract number 02E10790. The authors would like to thank  
400 Aline Chlupka and Stefanie Schubert for ICP-MS measurements, Carola Eckardt for BET  
401 determination, Heidrun Neubert for titration experiments as well as Andrea Scholz for XRD  
402 measurements.

## References

1. A. Fernández-Martínez and L. Charlet, *Rev. Environ. Sci. Biotechnol.*, 2009, **8**, 81-110.
2. F. Fordyce, *Ambio*, 2007, **36**, 94-97.
3. M. Navarro-Alarcon and C. Cabrera-Vique, *Science of the Total Environment*, 2008, **400**, 115-141.
4. S. Santos, G. Ungureanu, R. Boaventura and C. Botelho, *Science of the Total Environment*, 2015, **521-522**, 246-260.
5. G. Jörg, R. Buhnemann, S. Hollas, N. Kivel, K. Kossert, S. Van Winckel and C. L. V. Gostomski, *Applied Radiation and Isotopes*, 2010, **68**, 2339-2351.
6. E. J. Elzinga, Y. Z. Tang, J. McDonald, S. DeSisto and R. J. Reeder, *Journal of Colloid and Interface Science*, 2009, **340**, 153-159.
7. D. Laurenti, P. N. Bo, C. Roukoss, E. Devers, K. Marchand, L. Massin, L. Lemaitre, C. Legens, A. A. Quoineaud and M. Vrinat, *Journal of Catalysis*, 2013, **297**, 165-175.
8. M. Trueba and S. P. Trasatti, *European Journal of Inorganic Chemistry*, 2005, DOI: 10.1002/ejic.200500348, 3393-3403.
9. S. Koneti, L. Roiban, A.-S. Gay, P. Avenier, F. Dalmas and T. Epicier, *Microscopy and Microanalysis*, 2016, **22**, 58-59.
10. G. Lagaly and I. Dékány, in *Handbook of Clay Science*, Elsevier, Amsterdam, The Netherlands, Second edn., 2013, ch. 8.
11. T. Rabung, D. Schild, H. Geckeis, R. Klenze and T. Fanghänel, *Journal of Physical Chemistry B*, 2004, **108**, 17160-17165.
12. T. Kupcik, T. Rabung, J. Lützenkirchen, N. Finck, H. Geckeis and T. Fanghänel, *Journal of Colloid and Interface Science*, 2016, **461**, 215-224.
13. J. S. Yamani, A. W. Lounsbury and J. B. Zimmerman, *Water Research*, 2014, **50**, 373-381.
14. N. Loffredo, S. Mounier, Y. Thiry and F. Coppin, *Journal of Environmental Radioactivity*, 2011, **102**, 843-851.
15. C. H. Wu, S. L. Lo and C. F. Lin, *Colloids and Surfaces a-Physicochemical and Engineering Aspects*, 2000, **166**, 251-259.
16. D. Peak, *Journal of Colloid and Interface Science*, 2006, **303**, 337-345.
17. J. A. Ippolito, K. G. Scheckel and K. A. Barbarick, *Journal of Colloid and Interface Science*, 2009, **338**, 48-55.
18. C. P. Schulthess and Z. Q. Hu, *Soil Science Society of America Journal*, 2001, **65**, 710-718.
19. E. J. Boyle-Wight, L. E. Katz and K. F. Hayes, *Environmental Science & Technology*, 2002, **36**, 1212-1218.
20. S. Goldberg, *Soil Science Society of America Journal*, 2014, **78**, 473-479.
21. H. Wijnja and C. P. Schulthess, *Journal of Colloid and Interface Science*, 2000, **229**, 286-297.
22. P. M. Wang, A. Anderko and D. R. Turner, *Industrial & Engineering Chemistry Research*, 2001, **40**, 4444-4455.
23. M. M. Ghosh, C. D. Cox and J. R. Yuanpan, *Environmental Progress*, 1994, **13**, 79-88.
24. P. K. Glasoe and F. A. Long, *Journal of Physical Chemistry*, 1960, **64**, 188-190.
25. N. Jordan, H. Foerstendorf, S. Weiss, K. Heim, D. Schild and V. Brendler, *Geochimica et Cosmochimica Acta*, 2011, **75**, 1519-1530.

26. N. Jordan, K. Muller, C. Franzen and V. Brendler, *Journal of Colloid and Interface Science*, 2013, **390**, 170-175.
27. N. Jordan, A. Ritter, H. Foerstendorf, A. C. Scheinost, S. Weiss, K. Heim, J. Grenzer, A. Mucklich and H. Reuther, *Geochimica et Cosmochimica Acta*, 2013, **103**, 63-75.
28. N. Mayordomo, H. Foerstendorf, J. Lützenkirchen, K. Heim, S. Weiss, U. Alonso, T. Missana, K. Schmeide and N. Jordan, *Environmental Science & Technology*, 2018, **52**, 581-588.
29. T. Hiemstra, H. Yong and W. H. Van Riemsdijk, *Langmuir*, 1999, **15**, 5942-5955.
30. M. Bouby, J. Lützenkirchen, K. Dardenne, T. Preocanin, M. A. Denecke, R. Klenze and H. Geckeis, *Journal of Colloid and Interface Science*, 2010, **350**, 551-561.
31. J. C. Westall, *FITEQL: A Computer Program for Determination of Chemical Equilibrium Constants from Experimental Data*, Department of Chemistry, Oregon State University, Corvallis, OR, U.S.A., 1982.
32. E. P. Poeter and M. C. Hill, *Documentation of UCODE: A Computer Code for Universal Inverse Modeling*, 1998.
33. C. Dyer, P. J. Hendra, W. Forsling and M. Ranheimer, *Spectrochimica Acta Part A: Molecular Spectroscopy*, 1993, **49**, 691-705.
34. E. Laiti, P. Persson and L. O. Öhman, *Langmuir*, 1998, **14**, 825-831.
35. H. Wijnja and C. P. Schulthess, *Spectrochimica Acta Part A: Molecular and Biomolecular Spectroscopy*, 1999, **55**, 861-872.
36. G. Lefèvre, M. Duc, P. Lepeut, R. Caplain and M. Fédoroff, *Langmuir*, 2002, **18**, 7530-7537.
37. X. Carrier, E. Marceau, J. F. Lambert and M. Che, *Journal of Colloid and Interface Science*, 2007, **308**, 429-437.
38. K. Müller, H. Foerstendorf, V. Brendler, A. Rossberg, K. Stolze and A. Gröschel, *Chemical Geology*, 2013, **357**, 75-84.
39. G. Jegadeesan, K. Mondal and S. B. Lalvani, *Environmental Technology*, 2003, **24**, 1049-1059.
40. J. Lützenkirchen, T. Preocanin and N. Kallay, *Physical Chemistry Chemical Physics*, 2008, **10**, 4946-4955.
41. M. Kosmulski, *Surface Charging and Points of Zero Charge*, CRC Press 2009.
42. M. Kosmulski, *Journal of Colloid and Interface Science*, 2011, **353**, 1-15.
43. K. Nakamoto, *Infrared and Raman Spectra of Inorganic and Coordination Compounds. Part A: Theory and Applications in Inorganic Chemistry*, Wiley-Interscience, New York, Fifth edn., 1997.
44. C. M. Su and D. L. Suarez, *Soil Science Society of America Journal*, 2000, **64**, 101-111.
45. A. Olin, B. Noläng, E. G. Osadchii, L.-O. Öhman and E. Rosén, *Chemical thermodynamics of selenium.*, Elsevier, Amsterdam, 2005.
46. J. Lützenkirchen, R. Marsac, D. A. Kulik, T. E. Payne, Z. R. Xue, S. Orsetti and S. B. Haderlein, *Applied Geochemistry*, 2015, **55**, 128-137.
47. Z. M. Wang and D. E. Giammar, *Environmental Science & Technology*, 2013, **47**, 3982-3996.

## **SUPPORTING INFORMATION**

### **Uptake of selenium(VI) onto transition alumina**

Norbert Jordan<sup>1,\*</sup>, Carola Franzen<sup>1</sup>, Johannes Lützenkirchen<sup>2</sup>, Harald Foerstendorf<sup>1</sup>,  
David Hering<sup>3</sup>, Stephan Weiss<sup>1</sup>, Karsten Heim<sup>1</sup>, Vinzenz Brendler<sup>1</sup>

<sup>1</sup>Helmholtz-Zentrum Dresden - Rossendorf (HZDR), Institute of Resource Ecology, Bautzner  
Landstraße 400, 01328 Dresden (Germany)

<sup>2</sup>Institute for Nuclear Waste Disposal, Karlsruhe Institute of Technology, Hermann-von-  
Helmholtz Platz 1, 76344 Eggenstein-Leopoldshafen (Germany)

<sup>3</sup>current affiliation: sunfire GmbH  
Gasanstaltstraße 2, 01237 Dresden, Germany

\*Corresponding author:

Phone: +49 351 260 2148, e-mail: [n.jordan@hzdr.de](mailto:n.jordan@hzdr.de)

This supporting information contains 11 pages and 7 figures.

### XRD of raw transition alumina

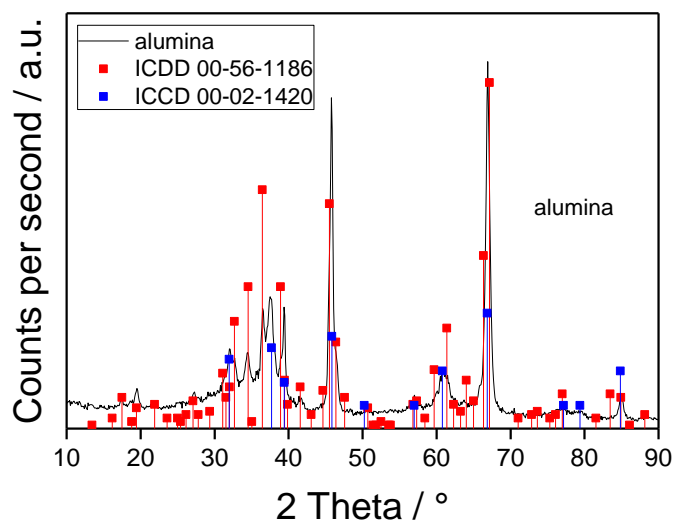


**Figure S1.** X-ray diffraction pattern of nano transition alumina at room temperature compared with the ICDD cards 00-056-1186 and 00-02-1420.

The  $\text{Al}_2\text{O}_3$  sample was characterized by XRD on a D8 Bruker-AXS diffractometer equipped with a graphite secondary monochromator, using  $\text{Cu K}\alpha$  radiation ( $\lambda = 1.5406 \text{ \AA}$ ) and operating in diffraction mode at 40 kV and 40 mA. Samples were step-scanned in the  $2\theta$  range of  $20\text{--}90^\circ$  in steps of  $0.05^\circ$  (15 s per step). By comparing the XRD patterns to the International Centre for Diffraction Data (ICDD) cards (Figure S1), the sample was identified as a polycrystalline phase mixture of  $\gamma\text{-Al}_2\text{O}_3$  (ICDD 00-002-1420) and  $\delta\text{-Al}_2\text{O}_3$  (00-056-1186) in a ratio of approximately 30:70.

**Effect of aging on the surface properties of transition-Al<sub>2</sub>O<sub>3</sub>**

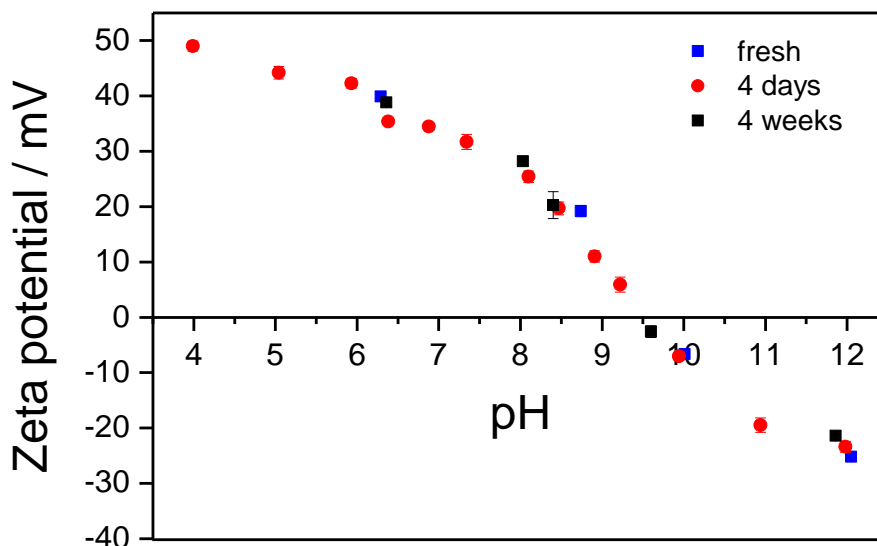


**Figure S2.** Zeta potential of transition alumina as a function of pH and time at 25 °C (m/v = 0.2 g·L<sup>-1</sup>, 0.1 mol·L<sup>-1</sup> NaCl).

Alumina was suspended in 50 mL polypropylene tubes in the presence of 40 mL of 0.1 mol·L<sup>-1</sup> NaCl solution (Merck, p.a.), yielding a mass to volume ratio m/v of 0.2 g·L<sup>-1</sup>. Samples were prepared in ambient air, since no impact of atmospherically derived carbonate on the zeta potential was observed in preliminary investigations. Suspensions were stirred and the pH values of the oxide suspensions were adjusted using either 0.1 or 0.01 mol·L<sup>-1</sup> HCl or NaOH. Each sample was ultrasonicated for 15 s with an ultrasonic finger (Sonopulse HD 2200, Bandelin) prior to measurements. An aliquot of approximately 1 mL was then transferred into a rectangular capillary cell made of polycarbonate with gold plated copper beryllium electrodes. A voltage of 50 V was applied across them. After 2 min of equilibration, the electrophoretic mobility of the suspension was measured at 25 °C. The measured velocity of the particle in the electric field was

converted to zeta potential using the Smoluchowski equation. The zeta potential was calculated with Zetasizer 6.01 software. The reported values were averaged over at least ten measurements.



### **Potentiometric titrations**

Potentiometric titrations (pH range 5 to 9.5) were performed at different ionic strengths of NaCl (0.1, 0.05 and 0.01 mol L<sup>-1</sup>) with a Metrohm 736 GP Titrino titrator. For each titration, a 30 g L<sup>-1</sup> suspension of nano transition alumina (50 mL volume) was inserted in a borosilicate vessel and equilibrated over night at pH ~5. A continuous argon flux (Argon N50 from Air Liquide) was applied over the suspension to minimize intrusion of atmospheric CO<sub>2</sub>. To ensure a homogeneous suspension, a Teflon propeller was used. After overnight pre-equilibration, titration by base was performed by addition of aliquots (20 μL) of 0.1 mol L<sup>-1</sup> NaOH. The pH electrode (Schott BlueLine 11pH) was calibrated using a three point calibration with buffer solutions (pH 4.01, 6.87 and 9.18).

**FT-IR studies**

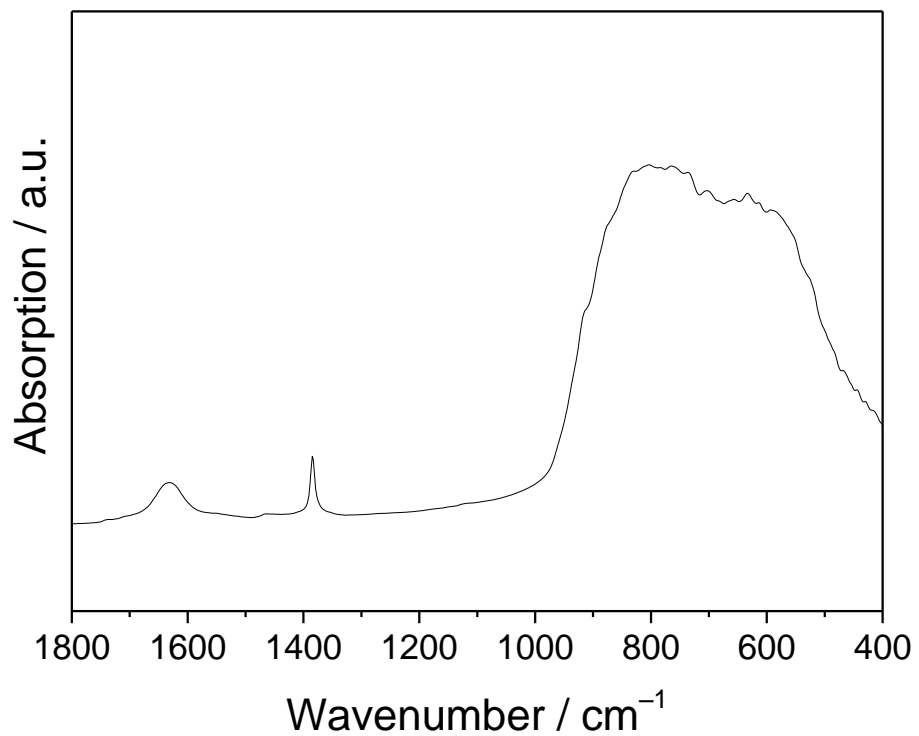


**Figure S3.** IR spectrum of transition alumina measured in a KBr matrix.

**IR spectra of Se(VI) sorption and desorption processes and dependence on ionic strength**

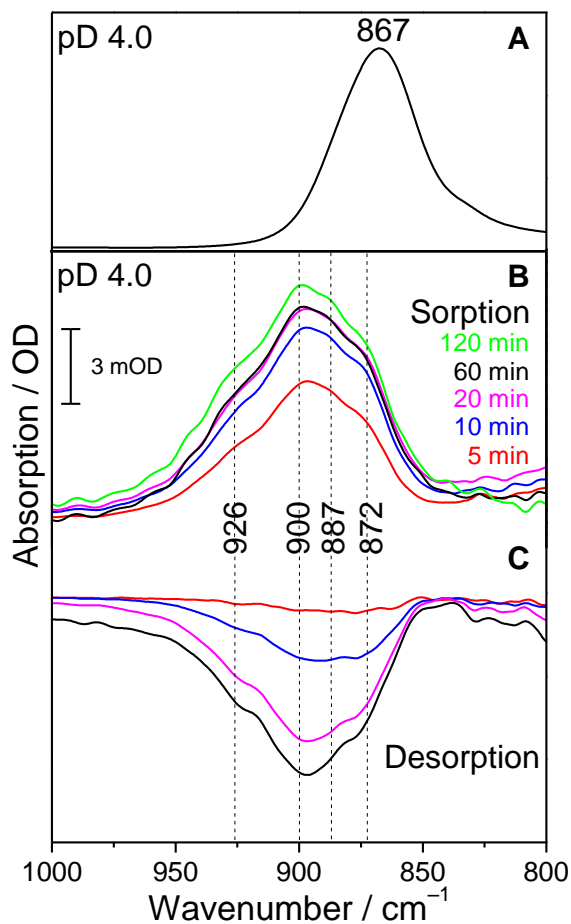


**Figure S4.** (a) IR spectrum of  $0.1 \text{ mol L}^{-1}$  selenium(VI) in aqueous solution at  $0.1 \text{ mol L}^{-1}$  NaCl in  $\text{D}_2\text{O}$ . (b) *In situ* IR spectra taken during selenium(VI) adsorption onto transition alumina ( $[\text{Se(VI)}]_{\text{initial}} = 5 \times 10^{-4} \text{ mol L}^{-1}$ ,  $\text{D}_2\text{O}$ , pD 4.0,  $0.1 \text{ mol L}^{-1}$  NaCl,  $\text{N}_2$ ) at different times. (c) *In situ* IR spectra during release of selenium(VI) at different times after starting to flush the transition alumina phase with blank solution ( $\text{D}_2\text{O}$ , pD 4.0,  $0.1 \text{ mol L}^{-1}$  NaCl,  $\text{N}_2$ ).

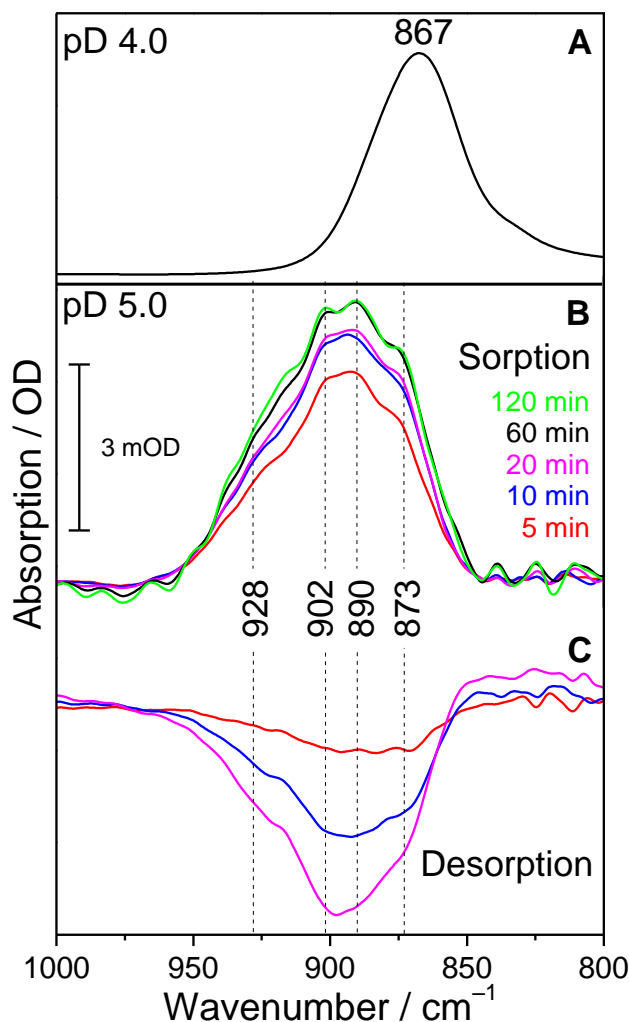


**Figure S5.** (a) IR spectrum of 0.1 mol L<sup>-1</sup> selenium(VI) in aqueous solution at 0.1 mol L<sup>-1</sup> NaCl in D<sub>2</sub>O. (b) *In situ* IR spectra taken during selenium(VI) adsorption onto transition alumina ([Se(VI)]<sub>initial</sub> = 5 × 10<sup>-4</sup> mol L<sup>-1</sup>, D<sub>2</sub>O, pD 5.0, 0.1 mol L<sup>-1</sup> NaCl, N<sub>2</sub>) at different times. (c) *In situ* IR spectra during release of selenium(VI) at different times after starting to flush the transition alumina phase with blank solution (D<sub>2</sub>O, pD 5.0, 0.1 mol L<sup>-1</sup> NaCl, N<sub>2</sub>).

The increase of the amplitudes after 60 minutes of induced sorption (Figure 5b) is only apparent because a continuous background drift occurred throughout the *in situ* experiment. This drift has an almost linear contribution to the spectra's amplitudes with time, thus, becoming obvious with

increasing acquisition time. In fact, already after 20 min the spectra did not show a significant increase of the amplitudes as can be derived from Figures S5c.

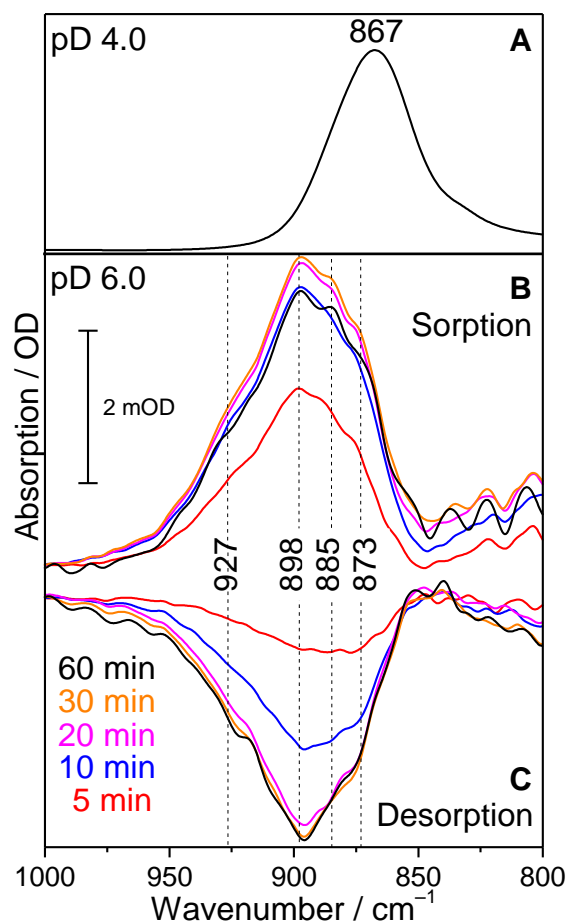


**Figure S6.** (a) IR spectrum of 0.1 mol L<sup>-1</sup> selenium(VI) in aqueous solution at 0.1 mol L<sup>-1</sup> NaCl in D<sub>2</sub>O. (b) *In situ* IR spectra taken during selenium(VI) adsorption onto transition alumina ([Se(VI)]<sub>initial</sub> = 5 × 10<sup>-4</sup> mol L<sup>-1</sup>, D<sub>2</sub>O, pD 6.0, 0.1 mol L<sup>-1</sup> NaCl, N<sub>2</sub>) at different times. (c) *In situ* IR spectra during release of selenium(VI) at different times after starting to flush the transition alumina phase with blank solution (D<sub>2</sub>O, pD 6.0, 0.1 mol L<sup>-1</sup> NaCl, N<sub>2</sub>).

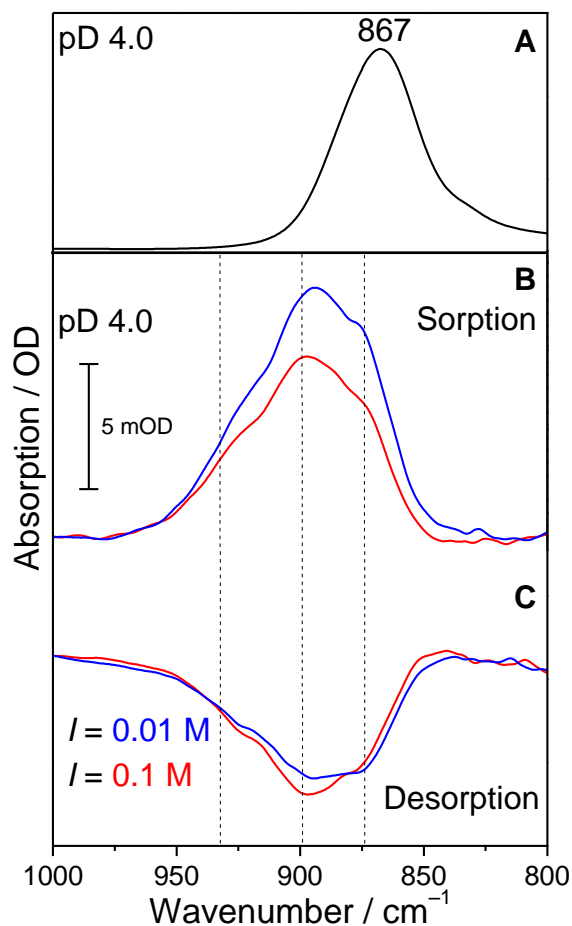


**Figure S7.** (a) IR spectrum of 0.1 mol L<sup>-1</sup> selenium(VI) in aqueous solution at 0.1 mol L<sup>-1</sup> NaCl in D<sub>2</sub>O. (b) *In situ* IR spectra taken during selenium(VI) adsorption onto transition alumina ([Se(VI)]<sub>initial</sub> = 5 × 10<sup>-4</sup> mol L<sup>-1</sup>, D<sub>2</sub>O, pD 4, 20 min of sorption, N<sub>2</sub>) recorded at different ionic strength. (c) *In situ* IR spectrum of release of selenium(VI) (D<sub>2</sub>O, pD 4.0, 20 min of desorption, N<sub>2</sub>) recorded at different ionic strength after starting to flush the transition alumina phase with blank solution.